Supplementary Information

Raman-encoded molecular imaging (REMI) with topically applied SERS nanoparticles for intraoperative guidance of lumpectomy

Yu "Winston" Wang[1,5*†], Nicholas P. Reder[1,2,†], Soyoung Kang[1], Adam K. Glaser[1], Qian Yang[1,4], Matthew A. Wall[1], Sara H. Javid[3], Suzanne M. Dintzis[2], Jonathan T.C. Liu[1*]

[1]Department of Mechanical Engineering, University of Washington, Seattle, WA 98195.
[2]Department of Pathology, University of Washington School of Medicine, Seattle, WA 98195.
[3]Department of Surgery, University of Washington School of Medicine, Seattle, WA 98195.
[4]Department of Pharmacy, Chengdu Medical College, Chengdu, Sichuan 615000, China.
* Corresponding author: Yu "Winston" Wang (Email: yuwang2@uw.edu), Jonathan T.C. Liu (Email: jonliu@uw.edu).
† These authors contributed equally to this work.

Study design

The objectives of this cross-sectional study were to assess the diagnostic accuracy of REMI for distinguishing benign breast tissue from carcinoma, and to demonstrate that imaging multiple cancer biomarkers enables sensitive tumor detection in the presence of significant inter-patient and intra-patient molecular heterogeneity. We calculated that we would need at least four positive cases and four negative controls for each biomarker to achieve power of 80% at an alpha level of 5%, assuming an AUC=0.95. Fifty-seven fresh specimens from 29 patients were imaged with REMI to simultaneously quantify the expression of four breast carcinoma biomarkers (HER2, membrane ER, EGFR and CD44), and to define the tumor regions. Patients were included in the study if they had a known diagnosis of either invasive carcinoma or ductal carcinoma in-situ. Exclusion criteria included stromal neoplasms, unknown diagnosis at the time of surgery, and small tumors (<1 cm) with insufficient residual tissue to offer for research (these tissues were completely submitted for clinical diagnosis). Study participants were prospectively enrolled, with informed consent, from November 2015 to October 2016. The study was stopped after achieving the desired sample sizes (n = 8 for HER2, n = 16 for ER, n = 15 for CD44, and n = 4 for EGFR, as listed in Supplementary Table S1).

After surgery, each specimen was topically stained with a mixture of 5 flavors of SERS NPs (4 targeted and 1 untargeted control) for 5 min and imaged at a spatial resolution of 0.5 mm and a raster-scanned imaging rate of >3 cm^2/min. The entire REMI procedure was performed within 10-15 min depending upon the size of the specimen, a time frame that is comparable to that of current intraoperative guidance techniques such as frozen-section analysis. The imaged specimens were processed for histological examination, randomized in order, and independently interpreted by two pathologists who were blinded to the REMI results (N.P.R and S.M.D). ROC analysis was performed to quantify the sensitivity, specificity, and overall accuracy for REMI to detect the overexpression of each of four biomarker targets, with immunohistochemistry (IHC) as the gold standard. To evaluate the overall sensitivity and specificity of REMI for the detection of breast carcinomas of any kind, in this early-stage study, we assumed that if one or more of the four candidate biomarkers was positively expressed in a region, then that tissue region should be considered malignant (Fig. 1). For tumor detection, H&E histology was used as a gold standard.

Review of prior studies to validate the technical robustness of REMI

1) Correlation of REMI with biomarker expression levels.
   Previous studies have been performed to demonstrate that the ratiometric results reported by REMI are linearly correlated with biomarker expression levels, as validated by flow cytometry. Therefore, REMI results may be considered a surrogate of biomarker expression levels (Supplementary Fig. S2) (1-4).

2) Optimization of topical staining protocols.
   Previous studies have been performed to optimize the concentration, staining duration, staining protocol, buffer composition, and NP conjugation protocols (1,4,5). A convection-enhanced topical staining method has been developed to enable rapid and reproducible imaging of 4 biomarkers in fresh tissue (4).

3) Optimization and validation of the negative-control SERS NP for ratiometric imaging.
   A negative-control SERS NP has been developed, in which isotype-matched antibodies are conjugated to the NPs. These negative-control NPs possess an identical geometry, surface charge, and nonspecific behavior with the targeted NPs that are conjugated to biomarker-specific monoclonal antibodies (5). Previous studies have been performed to demonstrate that the negative-control NPs served as a highly accurate control for nonspecific accumulation of NPs in cell lines, animal tissues and human tissues, enabling robust ratiometric imaging (1-3,5).

4) Optimization and validation of the accuracy of demultiplexing algorithms.
   Previous studies have been performed to optimize the least-squares-based demultiplexing algorithm and to demonstrate that the algorithm is highly accurate for quantifying multiplexed SERS NPs in tissues, even in the presence of background inks, hemoglobin, and intrinsic tissue-background components (2,4,6).

Selection of cell-surface biomarkers for REMI of breast tumors

The primary goal of REMI is to accurately identify residual breast tumors in as many patients as possible, and not to stratify patients for risk or treatment response. Therefore, the prevalence of the candidate biomarkers is of primary importance rather than their prognostic or oncologic

implications. HER2 is one of the most well studied transmembrane tyrosine kinase receptors, and is overexpressed in approximately 20 – 25% of breast cancers (7-9). While HER2 expression is associated with recurrent and aggressive breast cancers, the development of the humanized mAb trastuzumab (Herceptin) as a treatment for HER2-positive patients has dramatically improved their outcomes (9). Like HER2, another member of the epidermal growth factor receptor family that is overexpressed in certain breast cancer patients is EGFR, which has been associated with epithelial-mesenchymal transition (EMT), migration, and tumor invasion (10,11). In particular, EGFR has received much attention because it is overexpressed in a majority of patients with triple-negative breast cancer (i.e. lacking overexpression of HER2, estrogen receptor, and progesterone receptor). In the breast cancer community, CD44 has been extensively studied as a marker of breast cancer stem cells that are purported to exhibit a CD44(+)/CD24(-) phenotype (12,13). Recent studies have shown that CD44 expression is also prevalent in non-stem breast cancer cells and that it can be used as a biomarker to indicate risk of metastasis and aggressiveness, as well as to stratify patients (14,15). Estrogen receptors (ER) are overexpressed in >65% of breast-cancer patients, and have a significant influence on patient prognosis and treatment response (e.g. endocrine therapies) (16). While ER is primarily a nuclear marker, studies have shown that cell-membrane ER (mER) is also expressed by ER-positive tumor cells, but at a much lower level of expression (17,18). These studies have also shown that the genetic origins and protein epitopes of nuclear and membrane ER are identical, including both major sub-classes of ER (ERα and ERβ).

Spectral demultiplexing to quantify SERS NPs

A direct-classical-least-squares (DCLS) algorithm was employed to calculate the concentrations and ratios of various SERS NP flavors as described previously (1,2). In short, the acquired raw spectra were demultiplexed using the DCLS algorithm to calculate the weight of spectral components based on their reference spectra (e.g. reference spectra of the SERS NPs, the principal components of tissue-background spectra, etc.). The NP weights were then converted to NP concentrations based on calibration measurements with stock NPs of known concentrations. A high degree of measurement linearity for NP concentrations in the range of 1-400 pM has been demonstrated (Supplementary Fig. S1 and previous publications (2,4,5)). The NP concentrations

were used to calculate concentration ratios for ratiometric mapping (of specific vs. nonspecific NP accumulation). To calibrate the NP ratios, a 4-μL drop of the staining solution was positioned adjacent to the specimen(s) immediately prior to imaging, and was imaged together with the specimen(s).

Cell culture and flow cytometry for the validation of conjugated NPs

Four cell lines, including A431 (ATCC, CRL-1555), SkBr3 (ATCC, HTB-30D), MCF-7 (ATCC, HTB-22) and 3T3 (ATCC, CRL-1658), were used to validate the specific binding ability of conjugated NPs. A431, MCF-7 and 3T3 cells were cultured in DMEM medium (Lonza, 12-604F) and SkBr3 cells were cultured in Mccoy's 5A medium (Lonza, 12-688F), both of which were supplemented with 10% fetal bovine serum (FBS, Thermo Scientific, SH3008803) and 1% penicillin-streptomycin (Lonza, 17-602E). All cells were cultured at 37 °C with 5% CO_2. Trypsin EDTA (Mediatech, MT25051CI) was used to detach cells.

Flow cytometry samples were prepared by mixing 25-uL cell suspensions (0.2 million cells) with 25 μL of NP conjugates (150 pM) for 15 min at 20 °C with gentle agitation at 300 rpm, followed by three rounds of purification via centrifugation (400 g for 5 min) and supernatant-replacement (500 μL per rinse) with FACS buffer (1% BSA in PBS). Each cell line was split into equally sized samples that were individually stained by EGFR-NPs, HER2-NPs, ER-NPs, CD44-NPs or isotype-NPs. To ensure reproducible tissue imaging throughout the duration of this study, mAb-conjugated NPs were used for tissue imaging experiments only when they yielded flow-cytometry results that were similar (±20% error) to the ones shown in Supplementary Fig. S8.

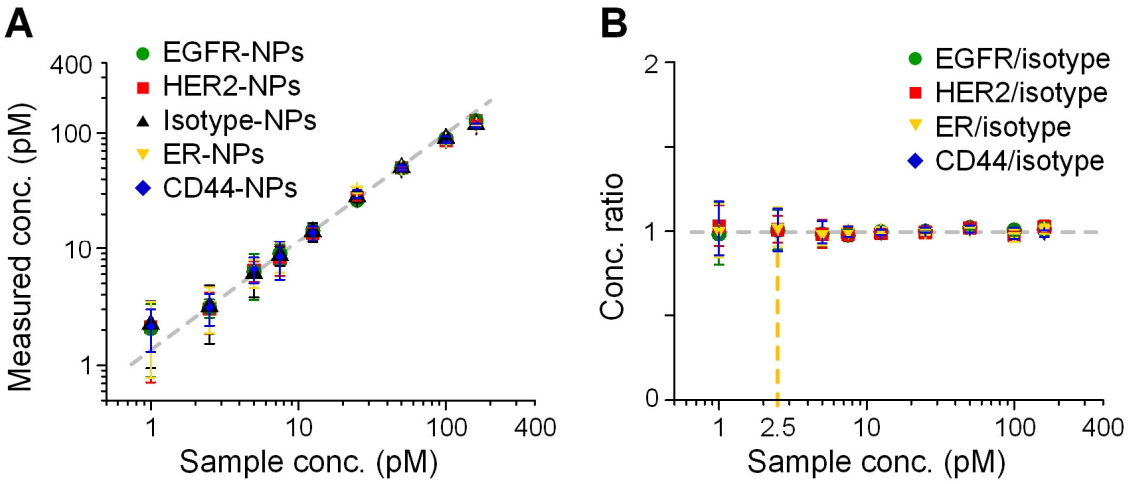

Supplementary Figure S1. Linearity and limit-of-detection of spectral measurements. Nine samples were prepared by mixing five NP flavors in an equimolar ratio and diluting the mixture to different concentrations. A 2-µL drop from each sample was placed on a piece of rat muscle, and 3 spectral measurements were acquired with the REMI system by directing the laser beam through the center of each drop. The acquired spectra (of the NP mixtures) were then demultiplexed to determine the individual NP concentrations (**A**) and the concentration ratios between the NPs (**B**). Since identical working distances (2 mm) and detection parameters was used for all measurements, absolute NP concentrations could be determined based upon calibration measurements with stock NPs of known concentrations. The error bars represent the standard deviation from multiple measurements. For this study, the limit-of-detection (2.5 pM marked with the orange dashed line) was defined as the NP concentration at which the error in the measured NP concentration ratios surpassed 15%. All data presented in this paper correspond to NP concentrations that are considerably greater than 2.5 pM (in a range of 12-160 pM).

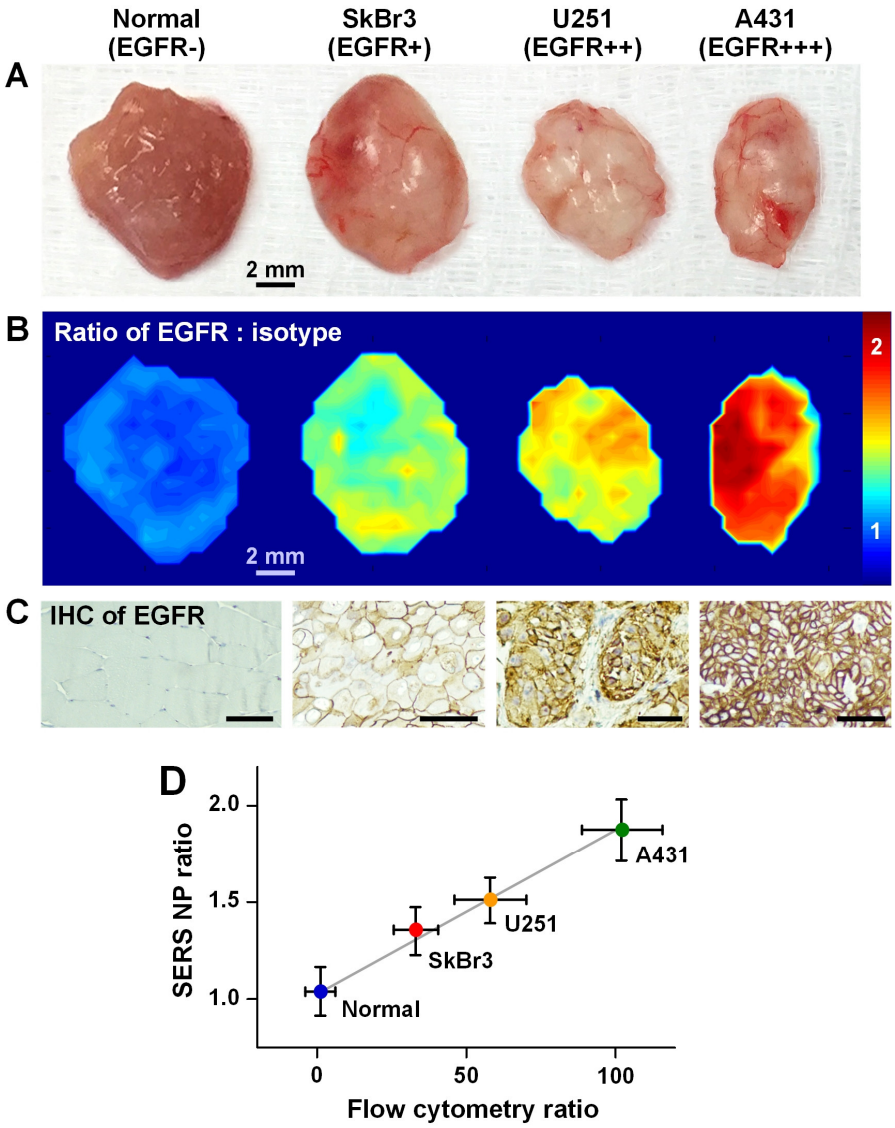

Supplementary Figure S2. REMI of normal tissue (EGFR-negative) and tumor xenografts (SkBr3, U251, and A431) that express various levels of EGFR. The tissue specimens were stained with a two-flavor NP mixture (EGFR-NPs and isotype-NPs, 150 pM/flavor) for 10 min, followed by raster-scanned imaging and spectral demultiplexing to simultaneously quantify the expression level of EGFR. The entire staining-and-imaging procedure was achieved in less than 15 min. **A**, Photographs of resected normal tissue (muscle) and tumor xenografts. **B**, Images of the concentration ratio of EGFR-NPs vs. isotype-NPs. The color bar indicates NP ratios. **C**, Validation data: IHC for EGFR. The scale bars represent 50 μm. **D**, Correlation between the REMI ratio of a particular tissue specimen (in **B**) and the corresponding fluorescence ratio (EGFR-NPs vs. isotype-NPs) from flow-cytometry experiments with the cell lines used to

generate the various tumor xenografts. R > 0.98. Flow cytometry results can be found in Fig. S4 and in our previous publication (1). The results in **B-D** demonstrate that REMI provides a quantitative measure of biomarker expression levels that agree with both gold-standard IHC and flow cytometry. All animal procedures were approved by the Institutional Animal Care and Use Committee (IACUC) at the University of Washington IACUC (#4345-01).

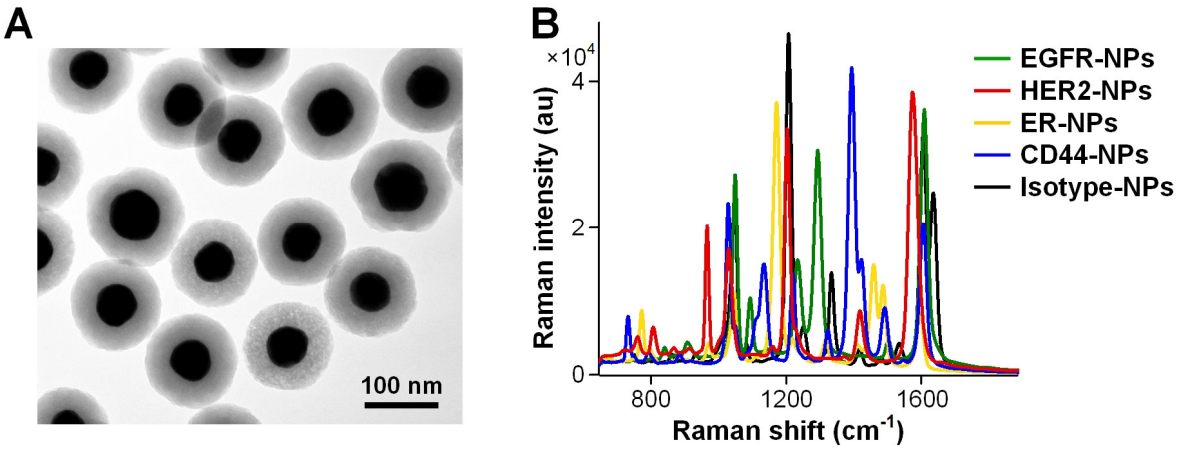

Supplementary Figure S3. Structure and spectra of SERS NPs. A, TEM image of SERS NPs. The gold cores of the NPs appear black, and are encapsulated by a silica shell that isolates the NP cores from the environment, as well as other NPs. This allows the NPs to generate a highly stable SERS signal that serves as a unique spectral fingerprint to identify each NP flavor. **B,** The reference spectra of the five NP flavors used in this study.

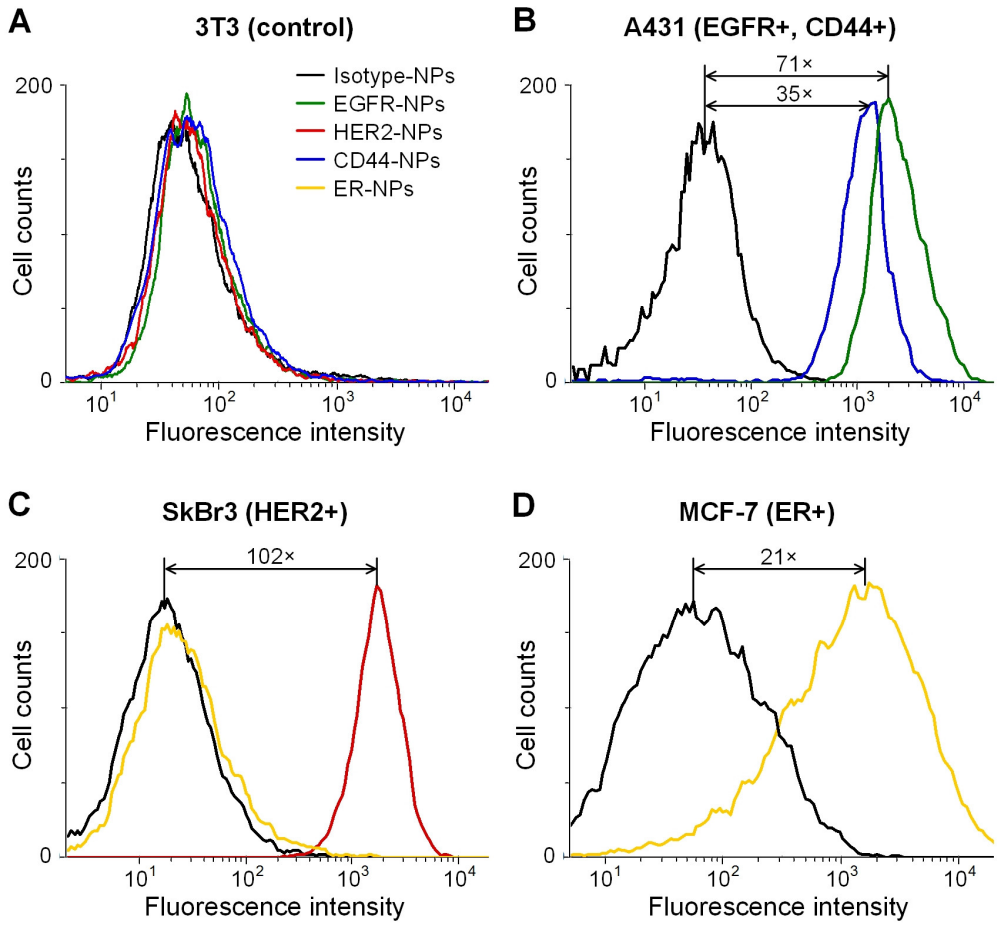

Supplementary Figure S4. Flow-cytometry based validation of the binding of targeted NPs to cell-surface receptors on cultured cells. EGFR-NPs, HER2-NPs, ER-NPs, CD44-NPs and isotype-NPs (150 pM) were individually used to stain (**A**) 3T3, (**B**) A431, (**C**) SkBr3 or (**D**) MCF-7 cell lines (15 min). Fluorescence histograms are shown from cells stained with isotype-control NPs or targeted NPs. 3T3 is a negative-control cell line for EGFR, HER2 and CD44, and SkBr3 is a negative-control cell line for ER. To ensure reproducible tissue imaging throughout the duration of this study, mAb-conjugated NPs were used for tissue imaging experiments only when they yielded flow-cytometry results that were similar (±20% error) to the ones shown in the plots.

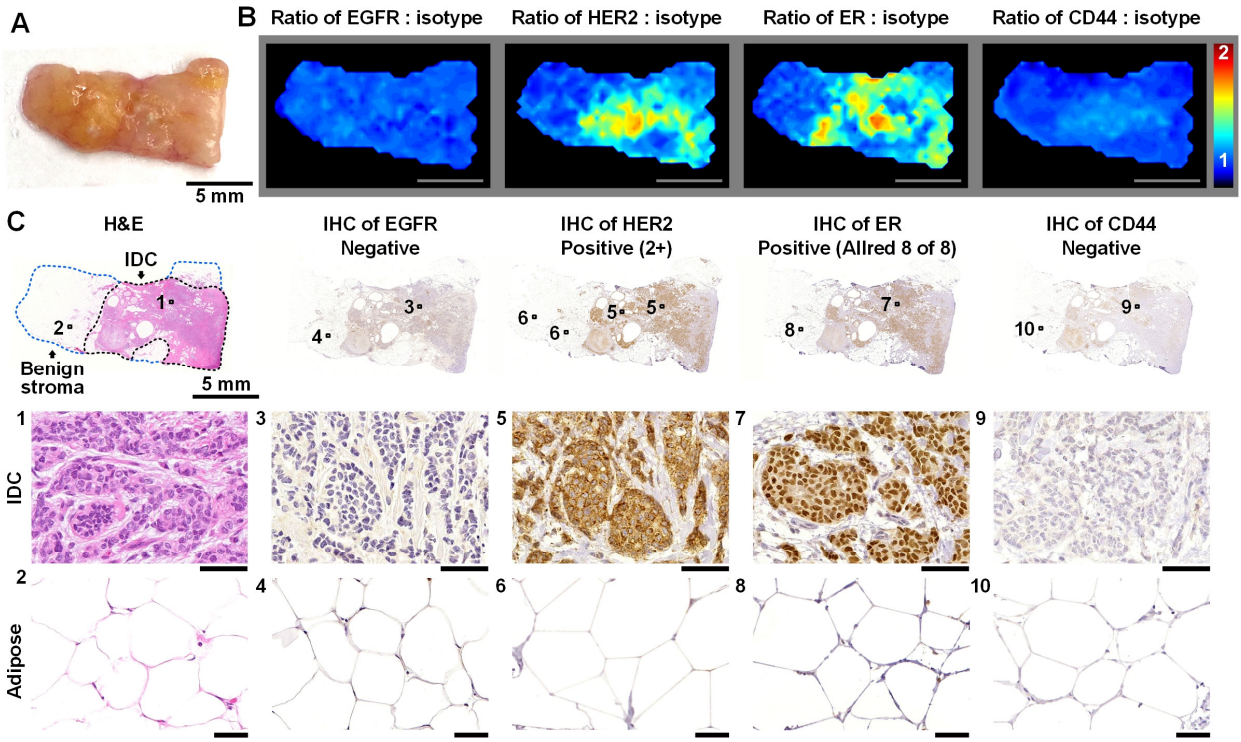

Supplementary Figure S5. REMI enables the detection of double-positive breast tumor (ER+ and HER2+). A, Photograph of a human breast specimen with ER+ and HER2+ IDC. **B,** REMI results. Unlabeled scale bars represent 5 mm. The color bar indicates NP ratios. **C,** Validation data: H&E and IHC. The specimen is positive for HER2 and ER, and negative for EGFR and CD44. Unlabeled scale bars represent 50 μm.

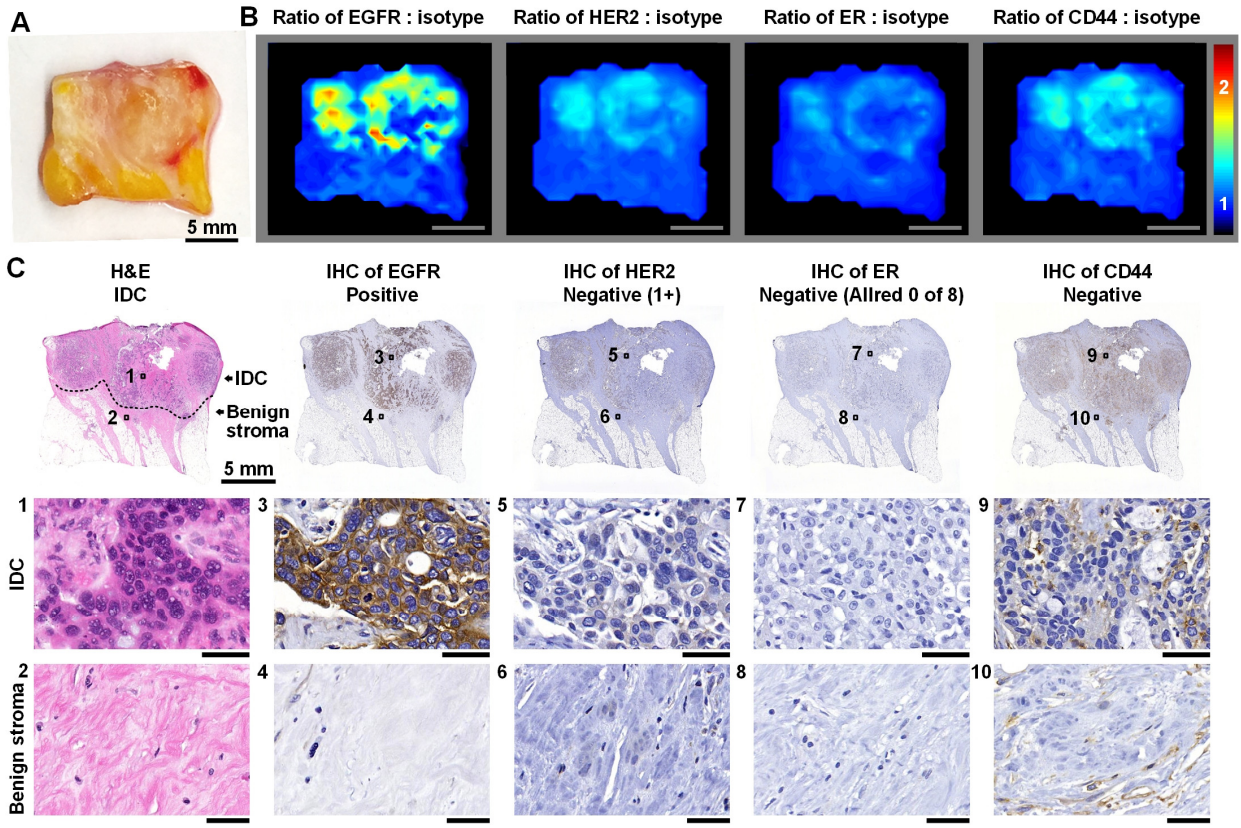

Supplementary Figure S6. REMI enables the detection of EGFR in a triple-negative breast tumor. A, Photograph of a human breast specimen with triple-negative IDC. **B,** REMI results. Unlabeled scale bars represent 5 mm. The color bar indicates NP ratios. **C,** Validation data: H&E and IHC. The specimen is positive for EGFR and negative for HER2, ER and CD44. Unlabeled scale bars represent 50 μm.

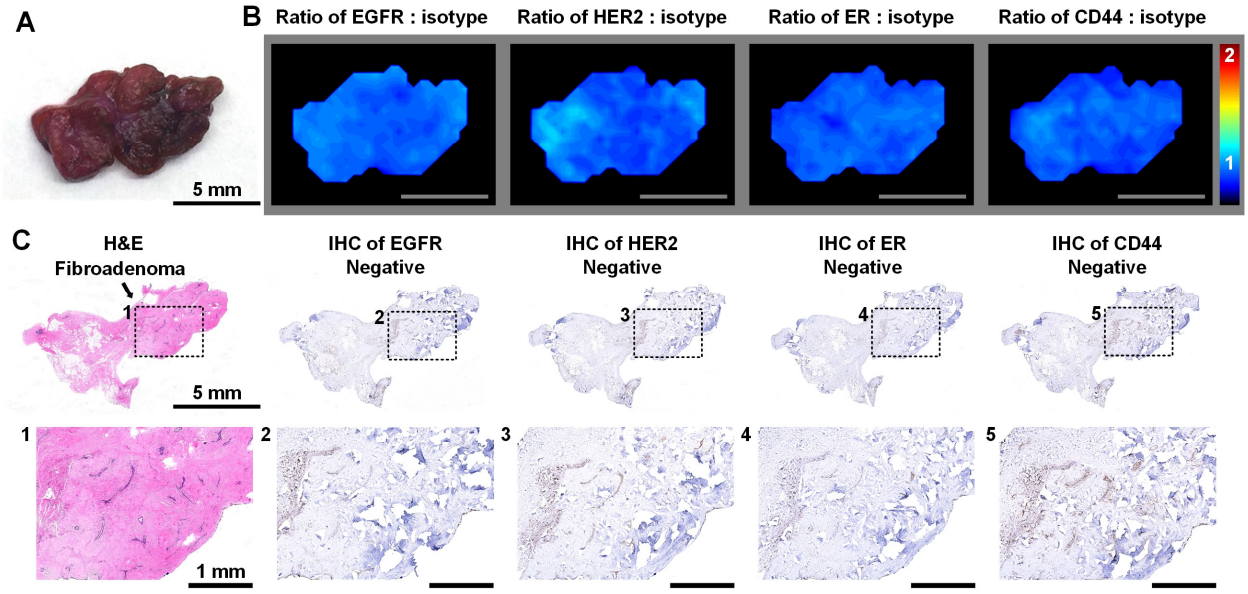

Supplementary Figure S7. REMI of fibroadenoma (benign lesion). A, Photograph of a human breast specimen with fibroadenoma. **B,** REMI reveals negligible expression of the 4 biomarkers. Unlabeled scale bars represent 5 mm. The color bar indicates NP ratios. **C,** Validation data: H&E and IHC. Inset 1 shows a fibroadenoma region. The specimen is negative for EGFR, HER2, ER and CD44, which agrees with the REMI results. Unlabeled scale bars represent 1 mm.

Supplementary Table S1. Benign lesions.

Benign lesion type	Number of patients	ROIs	Classified as benign
UDH	2	14	85.7%
Fibroadenoma	1	11	100%
Fibrocystic changes	4	46	91.3%
Total	7	71	91.5%

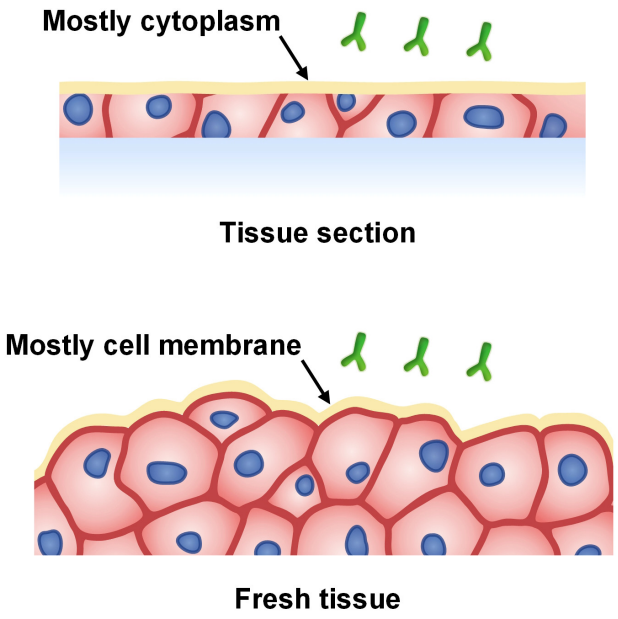

Supplementary Figure S8. An illustration of a key difference between staining histological tissue sections and fresh tissue surfaces. Thin (4-micron thick) histological tissue sections mostly display intracellular components (e.g. cytoplasm) within minimal presentation of the cell membranes. In contrast, for freshly excised tissue surfaces that have been stained and rinsed, the majority of the cells at the tissue surface are intact. Therefore, the large NPs, which are not rapidly internalized by cells, are mostly interacting/binding with the cell membranes and other extracellular proteins, rather than intracellular targets. Note that for surgically resected tissues, mucus and other competing materials are not a significant issue since staining and imaging are performed on the cut surfaces of the excised tissues. However, for topical staining and imaging of the GI tract, the mucus on the lumen surface can inhibit the effective delivery of SERS NPs to the tissue. In such cases, a mucolytic agent can be used prior to staining (3,6).

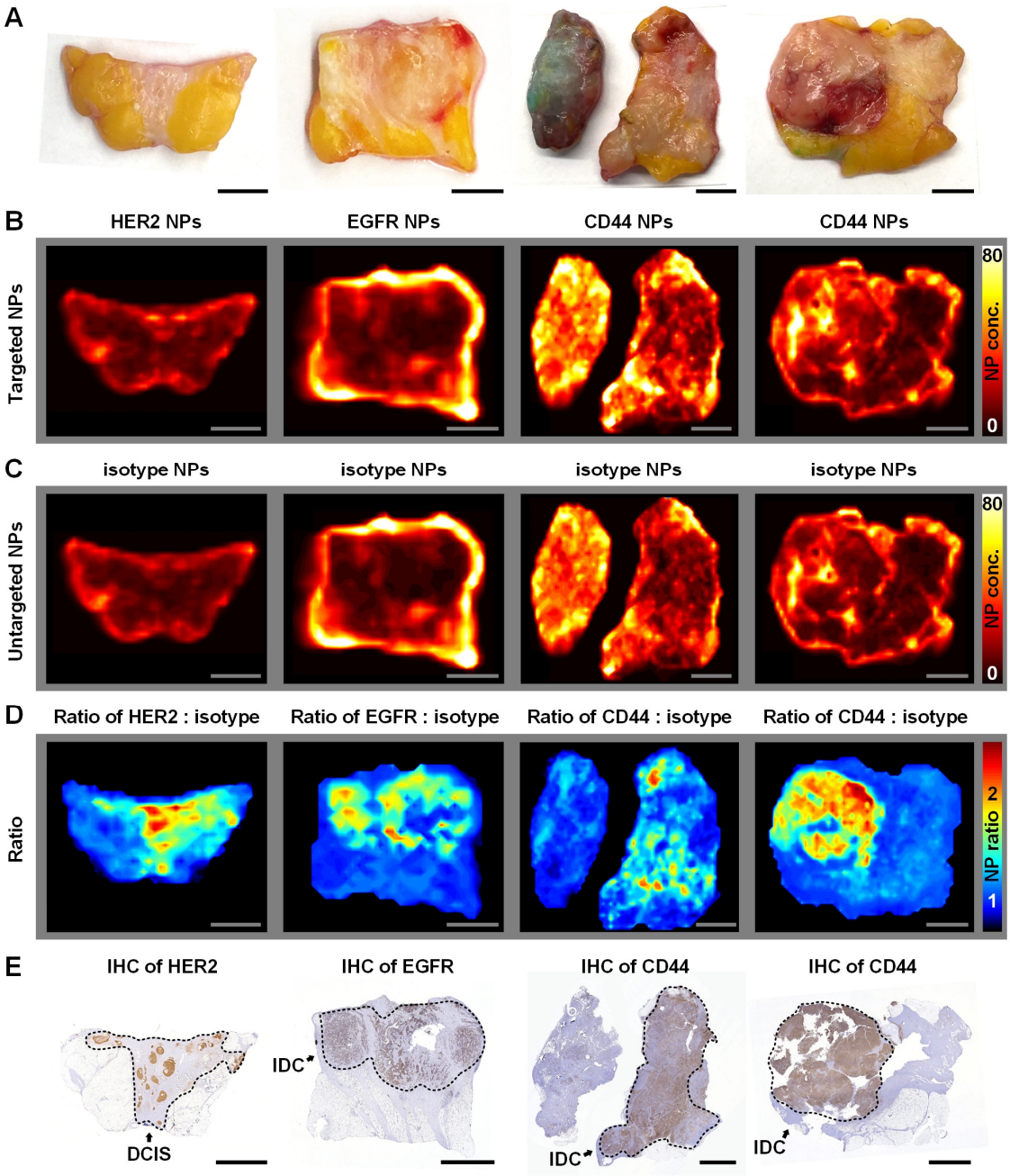

Supplementary Figure S9. Comparison of traditional single-targeted-agent imaging vs. ratiometric imaging, in which an untargeted agent is used to normalize for the nonspecific accumulation that occurs for all agents. A, Photographs of five tissue specimens from four patients. Images showing (**B**) the absolute concentration of targeted NPs, in which nonspecific accumulation of the NPs results in ambiguous results, and (**C**) the absolute concentration of untargeted NPs. (**D**) The concentration ratio of targeted NPs vs. isotype-NPs, which provides an accurate measure of specific vs. nonspecific NP retention in tissues that correlates with (**E**) IHC

validation data. The circled regions are positive for biomarker overexpression (based on gold-standard IHC). Scale bars represent 5 mm. An interesting result is shown in the third image in **B** in which all of the NP flavors administered on the specimens exhibited higher levels of overall accumulation on the benign specimen vs. the malignant specimen. This "inverse contrast" in the absence of ratiometric normalization, which was observed in this study as well as our previous studies(1,5), is partially due to the fact that the nonspecific accumulation of NPs is heavily influenced by the mechanical properties of a tissue, such as porosity and interstitial pressure, which are often higher in benign tissues compared with dense tumors (2,5,19). These types of nonspecific effects can generate misleading results for molecular imaging techniques in which a single targeted agent is administered and imaged (**B**), but are mitigated through the use of ratiometric imaging in REMI (**D**), in which a negative-control agent is used to normalize for the nonspecific accumulation of all of the contrast agents.

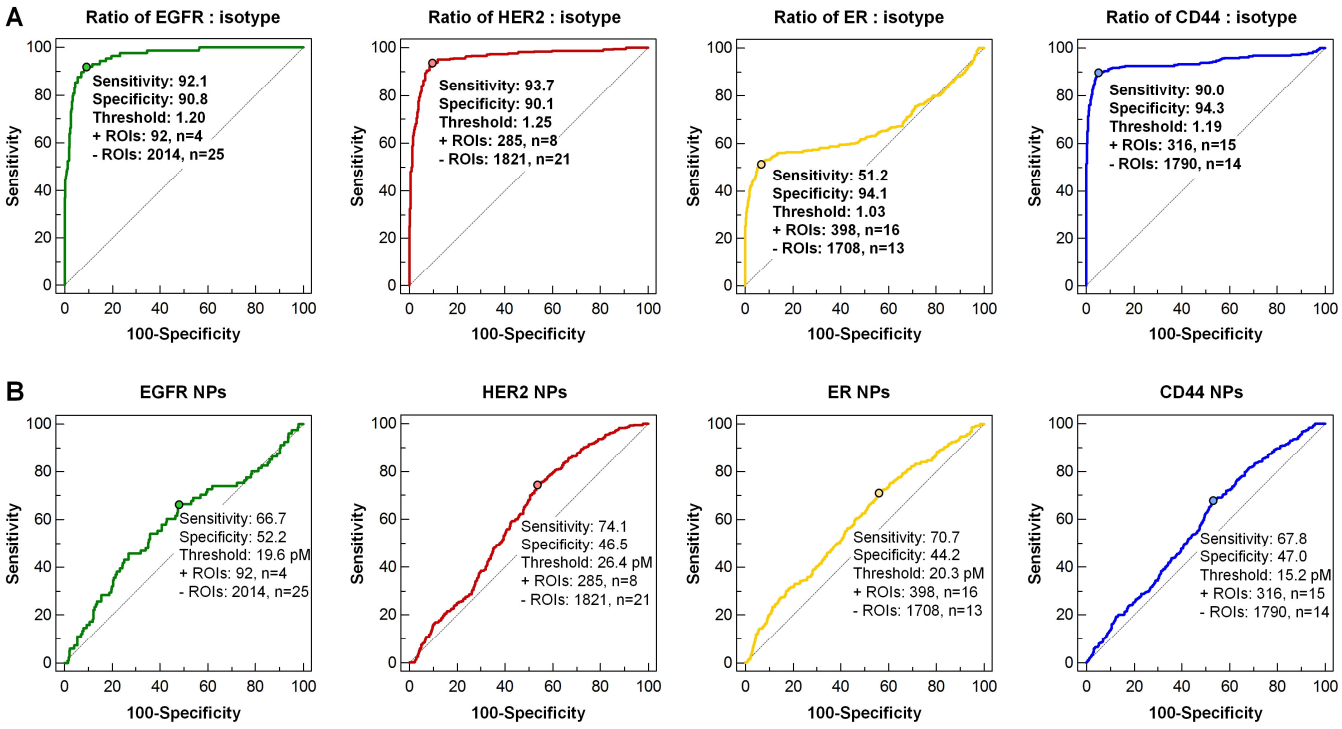

Supplementary Figure S10. Comparison of ROC curves for identification of biomarker expression using (A) a ratiometric imaging strategy (same as Fig. 5B) and (B) a traditional single-targeted-agent strategy. The ratio of targeted NPs vs. isotype-NPs from each of 2106 ROIs were used to generate the curves in **A**, and the concentration of targeted NPs alone were

used to generate the curves in **B**. IHC was used as the gold standard for identification of biomarker overexpression. (A) Ratiometric strategy: For the detection of EGFR overexpression, the area under the curve (AUC) = 0.96 with a 95% confidence interval (CI) of 0.96–0.97. For the detection of HER2 overexpression, the AUC = 0.96 with a 95% CI of 0.95–0.97. For the detection of mER overexpression, the AUC = 0.67 with a 95% CI of 0.64–0.69. For the detection of CD44 overexpression, the AUC = 0.94 with a 95% CI of 0.93–0.95. (B) Single-targeted-agent strategy: For the detection of EGFR overexpression, the area under the curve (AUC) = 0.58 with a 95% CI of 0.56–0.61. For the detection of HER2 overexpression, the AUC = 0.61 with a 95% CI of 0.59–0.63. For the detection of mER overexpression, the AUC = 0.60 with a 95% CI of 0.57–0.62. For the detection of CD44 overexpression, the AUC = 0.58 with a 95% CI of 0.55–0.60.

Supplementary Table S2. Molecular profile of patients.

Preoperative diagnoses	Number of patients	Molecular profile of resected tumor (IHC)	Number of patients	Malignant ROIs and sensitivity		Benign ROIs and specificity	
HER2 type	5	HER2+	3	111	93.7%	86	88.4%
		HER2+, CD44+	1	31	96.8%	43	86.0%
		HER2+, CD44+, EGFR+	1	21	100.0%	61	88.5%
Luminal A	16	ER+	6	107	54.2%	341	93.3%
		ER+, CD44+	7	146	95.9%	371	93.5%
		CD44+	3	67	91.0%	156	92.9%
Luminal B	3	ER+, HER2+	3	116	98.3%	176	89.2%
Triple negative	4	EGFR+	1	24	95.8%	34	91.2%
		EGFR+, CD44+	2	29	96.6%	83	92.8%
		CD44+	1	38	97.4%	42	95.2%
Benign Lesion	1	All -	1	-	-	23	95.7%
Total	29		29	690	89.3%	1416	92.1%

Supplementary References

1. Wang Y, Kang S, Khan A, Ruttner G, Leigh SY, Murray M, et al. Quantitative molecular phenotyping with topically applied SERS nanoparticles for intraoperative guidance of breast cancer lumpectomy. Sci Rep 2016;6:21242.
2. Wang Y, Kang S, Doerksen J, Glaser A, Liu J. Surgical Guidance via Multiplexed Molecular Imaging of Fresh Tissues Labeled with SERS-Coded Nanoparticles. IEEE J Sel Top Quantum Electron 2016;22(4):154-64.
3. Wang YW, Kang S, Khan A, Bao PQ, Liu JTC. In vivo multiplexed molecular imaging of esophageal cancer via spectral endoscopy of topically applied SERS nanoparticles. Biomed Opt Express 2015;6(10):3714-23.

4. Wang YW, Doerksen JD, Kang S, Walsh D, Yang Q, Hong D, et al. Multiplexed Molecular Imaging of Fresh Tissue Surfaces Enabled by Convection-Enhanced Topical Staining with SERS-Coded Nanoparticles. Small 2016;12(40):5612-21.
5. Wang YW, Khan A, Som M, Wang D, Chen Y, Leigh SY, et al. Rapid ratiometric biomarker detection with topically applied SERS nanoparticles. Technology (Singap World Sci) 2014;2(2):118-32.
6. Wang YW, Khan A, Leigh SY, Wang D, Chen Y, Meza D, et al. Comprehensive spectral endoscopy of topically applied SERS nanoparticles in the rat esophagus. Biomed Opt Express 2014;5(9):2883-95.
7. Engel RH, Kaklamani VG. HER2-positive breast cancer: current and future treatment strategies. Drugs 2007;67(9):1329-41.
8. Paik S, Bryant J, Tan-Chiu E, Yothers G, Park C, Wickerham DL, et al. HER2 and choice of adjuvant chemotherapy for invasive breast cancer: National Surgical Adjuvant Breast and Bowel Project Protocol B-15. J Natl Cancer Inst 2000;92(24):1991-8.
9. Slamon DJ, Leyland-Jones B, Shak S, Fuchs H, Paton V, Bajamonde A, et al. Use of chemotherapy plus a monoclonal antibody against HER2 for metastatic breast cancer that overexpresses HER2. N Engl J Med 2001;344(11):783-92.
10. Bhargava R, Gerald WL, Li AR, Pan Q, Lal P, Ladanyi M, et al. EGFR gene amplification in breast cancer: correlation with epidermal growth factor receptor mRNA and protein expression and HER-2 status and absence of EGFR-activating mutations. Mod Pathol 2005;18(8):1027-33.
11. Nielsen JS, Jakobsen E, Holund B, Bertelsen K, Jakobsen A. Prognostic significance of p53, Her-2, and EGFR overexpression in borderline and epithelial ovarian cancer. Int J Gynecol Cancer 2004;14(6):1086-96.
12. Phillips TM, McBride WH, Pajonk F. The response of CD24(-/low)/CD44+ breast cancer-initiating cells to radiation. J Natl Cancer Inst 2006;98(24):1777-85.
13. Sheridan C, Kishimoto H, Fuchs RK, Mehrotra S, Bhat-Nakshatri P, Turner CH, et al. CD44+/CD24- breast cancer cells exhibit enhanced invasive properties: an early step necessary for metastasis. Breast Cancer Res 2006;8(5):R59.
14. Honeth G, Bendahl P-O, Ringnér M, Saal LH, Gruvberger-Saal SK, Lövgren K, et al. The CD44+/CD24- phenotype is enriched in basal-like breast tumors. Breast Cancer Res 2008;10(3):1-12.
15. McFarlane S, Coulter JA, Tibbits P, O'Grady A, McFarlane C, Montgomery N, et al. CD44 increases the efficiency of distant metastasis of breast cancer. Oncotarget 2015;6(13):11465-76.
16. Anderson WF, Katki HA, Rosenberg PS. Incidence of breast cancer in the United States: current and future trends. J Natl Cancer Inst 2011;103(18):1397-402.
17. Pedram A, Razandi M, Levin ER. Nature of functional estrogen receptors at the plasma membrane. Mol Endocrinol 2006;20(9):1996-2009.
18. Soltysik K, Czekaj P. Membrane estrogen receptors - is it an alternative way of estrogen action? J Physiol Pharmacol 2013;64(2):129-42.
19. Tichauer KM, Samkoe KS, Sexton KJ, Gunn JR, Hasan T, Pogue BW. Improved tumor contrast achieved by single time point dual-reporter fluorescence imaging. J Biomed Opt 2012;17(6):0660011-06600110.